Defect-engineered optical bandgap in self-assembled TiO_2 nanorods on Si pyramids

C. P. Saini, A. Barman, B. Satpati, S. R. Bhattacharyya, D. Kanjilal, and A. Kanjilal'

Citation: Appl. Phys. Lett. **108**, 011907 (2016); doi: 10.1063/1.4939662
View online: http://dx.doi.org/10.1063/1.4939662
View Table of Contents: http://aip.scitation.org/toc/apl/108/1
Published by the American Institute of Physics

Defect-engineered optical bandgap in self-assembled TiO_2 nanorods on Si pyramids

C. P. Saini,[1] A. Barman,[1] B. Satpati,[2] S. R. Bhattacharyya,[2] D. Kanjilal,[3] and A. Kanjilal[1,a)]
[1]*Department of Physics, School of Natural Sciences, Shiv Nadar University, NH-91, Tehsil Dadri, Gautam Buddha Nagar, Uttar Pradesh 201 314, India*
[2]*Surface Physics and Material Science Division, Saha Institute of Nuclear Physics, 1/AF Bidhannagar, Kolkata 700 064, India*
[3]*Inter-University Accelerator Centre, Aruna Asaf Ali Marg, New Delhi 110 067, India*

(Received 13 November 2015; accepted 26 December 2015; published online 8 January 2016)

Transformation of self-assembled crystalline TiO_2 nanorods to amorphous layer, and the corresponding impact on optical-bandgap (E_g) on Si pyramids are investigated by irradiating with 50 keV Ar^+-ions. Initially, E_g is found to be reduced from 3.23 to 2.94 eV up to a fluence of 1×10^{16} ions/cm^2, and discussed in terms of the rise in oxygen vacancies (V_O). However, a sudden increase in E_g to 3.38 eV is detected at a fluence of 1×10^{17} ions/cm^2 through evolution of voids by over-saturating V_O, manifesting the appearance of degenerate states by shifting the Fermi level above the conduction band minimum via Burstein-Moss effect. © *2016 AIP Publishing LLC*.
[http://dx.doi.org/10.1063/1.4939662]

Bandgap tuning of metal oxides is not only a fundamental topic of materials research, but also important for (opto) electronic applications that include light harvesting, photocatalysis, gas sensing, etc.[1] Among various metal oxides, TiO_2 has attracted immense interest due to its ability to minimize the electron-hole recombination losses during photocatalytic process,[2] along with nontoxicity, chemical stability, and low production cost.[2,3] The efficient photocatalytic effect, however, demands matching of the TiO_2 conduction band (CB) with the redox-potential of water, which in turn leads to the removal of organic pollutants/impurity from water and also for producing hydrogen via water splitting.[2,4] But, the performance is dictated by the polymorphs, namely, thermodynamically stable rutile (R-TiO_2) and metastable anatase (A-TiO_2) structures with an average bandgap of ~3 and 3.2 eV, respectively.[5,6] The situation can be improved with increasing surface-to-volume ratio by producing nanostructures.[7] Except ultraviolet (UV) radiation, they have limited contribution to the visible range of solar spectrum, and therefore require engineering optical bandgap for large scale application.

This can be achieved through the development of sub-bandgap states either by doping with foreign elements[8] or by artificially introducing structural defects like Ti-interstitials and/or oxygen vacancies (V_O).[1,9] For instance, it was shown that the optical bandgap of TiO_2 can be reduced by introducing intermediate defect states, mostly associated with the evolution of V_O via modifying the structure.[3] Annealing temperature driven tuning of bandgap has also been reported and expressed in the light of local engineering of V_O.[10] It was, however, shown recently that the Ti-3d derived state (originated via removal of twofold surface bridging oxygen) can be situated at ~0.85 eV below the Fermi level due to the transfer of two excess electrons per V_O to nearby Ti atoms,[11] though the distributions of V_O is significantly different in R-TiO_2 and A-TiO_2 phases.[5] This is due to the diffusion of Ti interstitials towards the surface in the former case,[11] while V_O residing in the bulk of A-TiO_2 are energetically favorable than that of surface as the formation energy of V_O at the surface dominates over bulk by ~0.5 eV (Refs. 12 and 13) and thus makes the surface highly reactive.[14] Ion beam irradiation is promising in this respect due to its ability to produce and control the distribution of V_O in a predetermined depth by appropriate choice of ion species, energy, and fluence (i.e., ions/cm^2).[15] In particular, energetic Ar^+ ions have attracted a considerable interest not only for developing nanoripples on TiO_2 surfaces,[16] but also for modifying the structure to tune optical properties of TiO_2.[17] We further demonstrated the efficacy of Ar^+-ions in realizing TiO_2-based resistivity switching devices by introducing V_O.[18] However, Pabón *et al.* showed a clear transformation of TiO_2 into a single crystalline TiO film by Ar^+-ion irradiation.[17] Despite various application of Ar^+-ion irradiated TiO_2 layers, detailed exploitation of the structure and chemical properties for light harvesting in silicon solar cells by reducing the reflection loss[19] as a function of fluence is still lacking. This is also desirable on textured Si surfaces as they act as a potential platform for minimizing the reflection loss.[20]

In this letter, we show how optical bandgap of self-organized TiO_2 nanorods (NRs) on Si pyramids can be modified by Ar^+-ion bombardment, while it provides *degenerate states* at a critical fluence of 1×10^{17} ions/cm^2 due to the shift in Fermi level (E_F) into the CB according to Burstein-Moss (B-M) effect.[21,22]

To reveal the phenomenon, ultrasonically cleaned pieces of 500 μm thick p-type Si(100) wafers (area 1×1 cm^2) were initially chemically etched for achieving self-assembled pyramids (details in Ref. 20), which act as templates for growing TiO_2 layers. About 70 nm thick TiO_2 was deposited on Si pyramids at room temperature (RT) by 100 W RF sputtering (Excel Instruments) using a 6 mm thick 2 in. TiO_2 target (MTI corp., purity 99.99%). The substrate-to-target

a)Author to whom correspondence should be addressed. Electronic mail: aloke.kanjilal@snu.edu.in

distance was kept at 13 cm, while substrate rotational speed was of 9 rpm for achieving a uniform TiO_2 film. Highly pure (99.999%) oxygen and Ar gases were purged into the vacuum chamber (base pressure $\sim 1 \times 10^{-7}$ Torr) with a rate of 12 sccm and 30 sccm, respectively, for maintaining a working pressure of 8 mTorr.

The penetration depth of ions and the vacancy distribution in TiO_2 layers were studied by Stopping and Range of Ions in Matter (SRIM) calculations[23] when bombarded at an angle of 45° from the surface normal to comply with real situation. A typical vacancy distribution is shown in Fig. S-1.[24] After selecting the ion beam energy from SRIM calculations, the as-grown TiO_2 layers (called S_0) were irradiated at RT under normal incidence by 50 keV Ar^+-ions with a beam current of 1 μA and fluences in the range of $(0.05–10) \times 10^{16}$ ions/cm^2. The samples irradiated with fluences of 5×10^{14}, 1×10^{15}, 1×10^{16}, and 1×10^{17} ions/cm^2 are called by S_1, S_2, S_3, and S_4, respectively, in the following. The surface morphologies of textured Si surfaces before and after TiO_2 deposition, followed by ion beam exposure were investigated by scanning electron microscopy, SEM (Carl Zeiss). The thickness of the TiO_2 films was estimated by stylus profilometer with a resolution of 0.5 nm (Bruker, DektakXT), where crystalline phases were identified by glancing-incidence x-ray diffraction, GXRD (Bruker, D8-Discover) using a Cu-K_α radiation ($\lambda = 0.154$ nm) at an incidence angle of 0.5° and over a 2θ scan range of 20°–70°. The diffuse reflectance spectra were recorded by an integrating sphere attached in a Ultraviolet-Visible-Near-infrared (UV–VIS–NIR) spectrophotometer (Shimadzu Solid-Spec-3700). Microstructures of the selective samples were examined by 300 keV FEI Tecnai G^2 S-Twin transmission electron microscopy (TEM). Surface chemical analyses were carried out using a Mg-K_α ($\lambda = 9.89$ Å) source in an XPS system (VSW, Ltd., UK) integrated with a hemispherical analyzer.[18] Calibration of binding energy (BE) scale was made using gold Fermi edge.

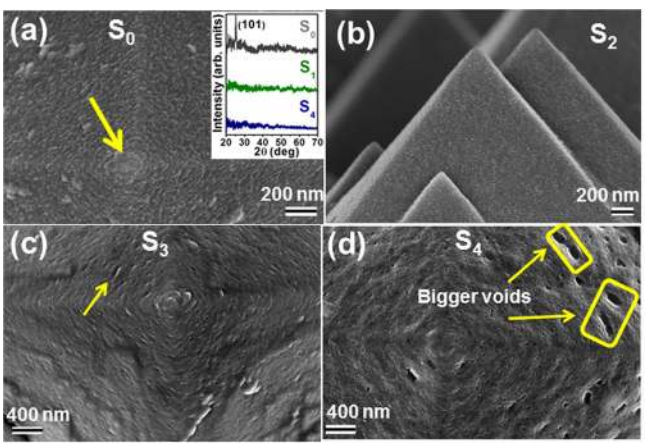

FIG. 1. (a) Magnified plan-view SEM image of granular TiO_2 layer on a Si pyramid (S_0), while the inset represents the GXRD patterns of before (S_0) and after ion-irradiation with fluences of 5×10^{14} (S_1) and 1×10^{17} ions/cm^2 (S_4). Magnified SEM images of the TiO_2 layer irradiated with a fluence of 1×10^{15} ions/cm^2 in cross-sectional geometry (b), and with fluences of 1×10^{16} ions/cm^2 (c) and 1×10^{17} ions/cm^2 (d) in plane-view geometry. The void-like structure for S_3 is shown by a yellow arrow in (c), while the formation of bigger voids near the valley region of S_4 are marked by rectangular boxes in (d), indicating evolution of voids with increasing ion fluence.

Plan-view SEM image of TiO_2 just after deposition on a typical Si pyramid[20] is exhibited in Fig. 1(a), showing formation of nanoscale grains, where a downward arrow indicates the pyramid apex. Moreover, the evolution of anatase-TiO_2 (A-TiO_2) in S_0 was detected from GXRD analyses, showing a preferential orientation of grains that give a dominant reflection from the (101) crystalline planes at 2θ of ~25.3° [inset, Fig. 1(a)]. As is clear from the inset of Fig. 1(a) that the crystalline TiO_2 layer was amorphized with increasing ion fluence, though a granular structure was evident up to an ion fluence of 1×10^{15} ions/cm^2 in S_2 [Fig. 1(b)]. With further increase in ion fluence, a clear change in morphology was noticed. For instance, grains in the S_3 surface were completely disappeared by setting up pore-like features where one of them is marked by an arrow [Fig. 1(c)]. These pores were found to increase in size and density in S_4, though they were mostly accumulated near the valley regions as the ones indicated by rectangles [Fig. 1(d)].

To follow the fluence dependent change in morphology, detailed microstructural study has been carried out by TEM in cross-sectional geometry (XTEM). Comparing the granular structures of S_0 [Fig. 1(a)], a magnified XTEM image of the same illustrates the formation of randomly oriented TiO_2 NRs with an average length and width of ~65 and 15 nm, respectively, within an error of ±10% [Fig. 2(a)]. The distribution of such self-assembled NRs is governed by the initial nucleation sites on Si facets, followed by the growth of one-dimensional structure via diffusion of adatoms depending on the growth parameters like substrate temperature, adatom's energy, deposition rate, etc.[25] Close inspection near the TiO_2/Si interface, however, reveals the evolution of a buffer layer prior to the growth of TiO_2 NRs. High resolution TEM (HRTEM) image of the dashed-rectangular region in Fig. 2(a) suggests the development of crystalline TiO_2 NRs from an amorphous buffer layer on a very thin ($\sim 2 \pm 0.5$ nm) native SiO_x layer [Fig. 2(b)]. The origin of SiO_x layers can be associated with the diffusion of oxygen radicals during the growth of TiO_2 film.[26] Moreover, XTEM image of S_3 recommends a clear transformation of the crystalline TiO_2 NRs (in S_0) to an amorphous layer with an average thickness of about 45 nm [Fig. 2(c)], though subsequent energy-filtered TEM (EFTEM) image [Fig. 2(d)] hardly gives any signature of Ti diffusion in Si matrix and vice versa. Since the ion beam plays a crucial role in modifying the stoichiometry by breaking the Ti-O bonds, it can promote the formation of a TiO_x layer with n-type conductivity in the presence of V_O. The HRTEM image in Fig. 2(e) further advocates a complete destruction of crystalline NRs followed by development of a rough SiO_x layer at the TiO_x/Si interface with an average thickness of ~6 nm. We believe that the O atoms during ion bombardment can diffuse through the TiO_2 matrix and form additional SiO_x through reaction with the surface Si atoms.

With further increase in ion fluence (i.e., 1×10^{17} ions/cm^2), voids are formed in the TiO_x layers on Si facets as evidenced in S_4 [Fig. 2(f)]. Close inspection, however, shows that the underneath crystalline Si substrate (c-Si) becomes amorphous (a-Si) up to a depth of ~25 nm from the Si surface. Detailed XTEM analyses [Fig. 2(g)] suggest the formation of bigger voids near the valley region, in agreement with the SEM results [see Fig. 1(d)]. The HRTEM image of

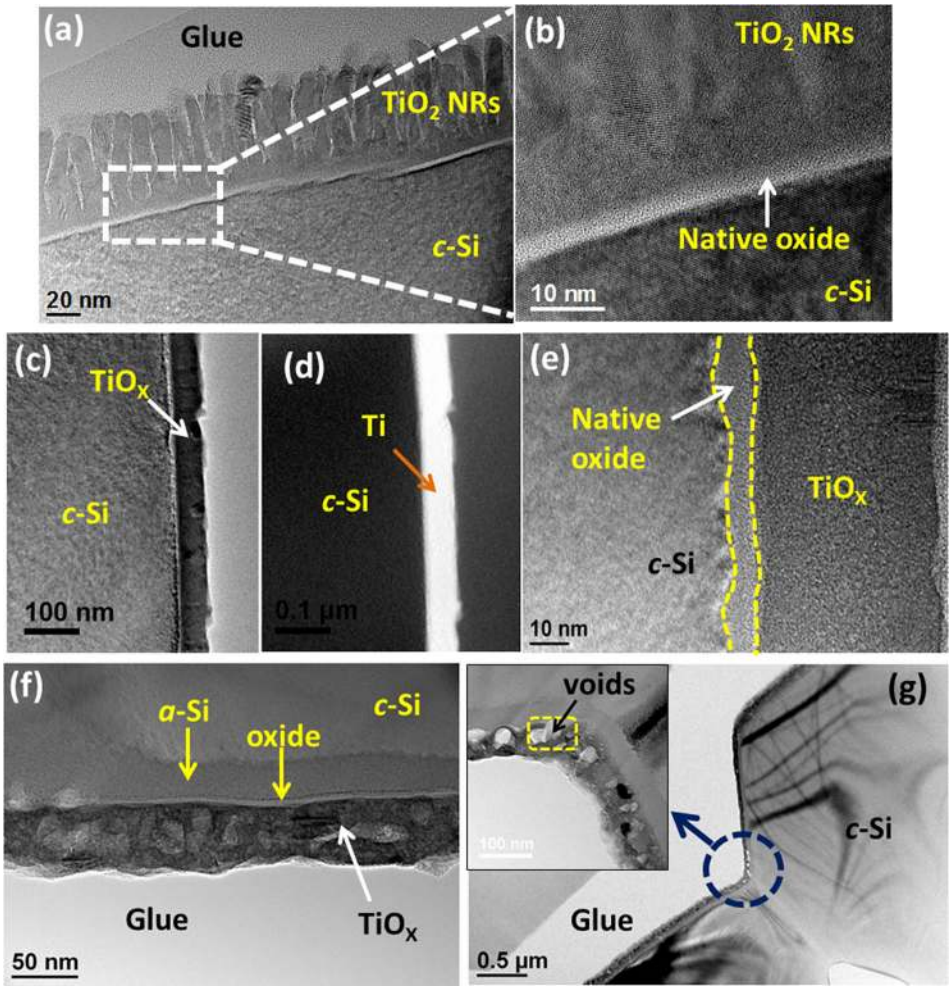

FIG. 2. (a) XTEM image of S_0, showing the formation of TiO_2 NRs on the facet of a Si pyramid; (b) HRTEM image of the white dashed rectangular region in (a), showing the formation of crystalline TiO_2 NRs from an amorphous buffer layer on a very thin native SiO_x layer. (c) Bright-field XTEM image of S_3, while the corresponding EFTEM and HRTEM images are exhibited by (d) and (e), respectively, showing a clear transformation from crystalline NRs to amorphous layer. The dashed yellow lines in (e) represent the native oxide layer. (f) Magnified XTEM image of a facet of S_4, showing the formation of voids in the TiO_x layer and the transformation of the surface region of the underneath crystalline Si to amorphous layer up to a depth of ~25 nm. (g) XTEM image of S_4, indicating the development of voids in the valley regions of Si pyramids, while they are prominent in the HRTEM image, as shown in the inset.

the dashed circle region further confirms the construction of voids in the range of 25–30 nm [marked by dashed rectangle in the inset of Fig. 2(g)] which are most likely occurred due to the over-saturation of V_O. This in turn gives an oxygen-deficient layer with an average stoichiometry of $TiO_{1.13}$ as revealed from energy-dispersive x-ray spectroscopy, EDS, studies (not shown).

Due to opaque nature of the underneath Si substrate, diffuse reflectance (R_D) has been monitored to follow the change in optical bandgap of TiO_2 as a function of fluence. The recorded R_D was analyzed by Kubelka-Munk (K-M) theory for any wavelength[8,27] $F(R_D) = \frac{(1-R_D)^2}{2R_D}$, where $F(R_D)$ is the K-M function,[8] which can further be expressed for TiO_2 with indirect bandgap as $\left[\frac{F(R_D)h\nu}{t}\right] = A(h\nu - E_g)^2$. Here, A is a constant and t is the layer thickness. Since the valance band (VB) and CB of TiO_2 are associated with the O-2p and Ti-3d states, respectively,[28] initially R_D of S_0 has been measured [Fig. 3(a)] to confirm the dominant role of anatase phase with an optical bandgap of 3.22 eV.[6,29] Clearly, any modification in BE of the O-2p and Ti-3d states due to the rearrangement of Ti and O atoms can bring change in the bandgap as the one evidenced in rutile-TiO_2 (3.0 eV).[6] This can be achieved also by introducing defects.[13,30] As the UV-VIS-NIR is considered to be a powerful technique for measuring the optical bandgap, this was employed to follow the impact of energetic ions in regulating bandgap of TiO_2 with increasing fluence. As expected, the bandgap is reduced from 3.23 to 2.94 eV up to a fluence of 1×10^{16} ions/cm^2 [Figs. 3(a) and 3(b)] where the observed phenomenon can be attributed to the appearance of sub-bandgap states due to the evolution of oxygen-deficient centers via breaking bonds of TiO_2, in good agreement with the previous reports.[2] Considering effective area of modification mainly due to

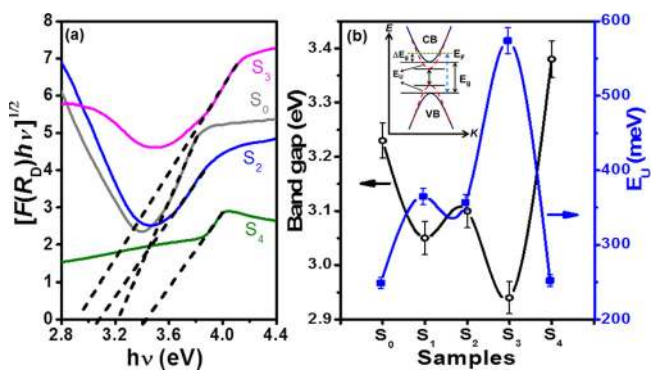

FIG. 3. (a) Kubelka-Munk function of the defused reflectance, showing the $[F(R_D)h\nu]^{1/2}$ versus incident photon energy ($h\nu$) plots for S_0, S_2, S_3, and S_4; determined optical bandgaps by fitting the absorption coefficients (for indirect material) through linear extrapolation in Tauc method. (b) Left ordinate (black) projects a trend of optical bandgap with increasing fluence, while right ordinate (blue) represents the corresponding change in Urbach energy (E_U); the inset gives a schematic representation of E_U and shifting of E_F in degenerated states having a width of ΔE_g.

elastic collision at this energy as ~1 Å^2 (~10^{-16} cm^2), there will be about 10 times more overlap at a fluence of 1×10^{17} ions/cm^2 in the modified regions causing the evolution of voids though accumulation of V_O after amorphization at the fluence of 1×10^{16} ions/cm^2. Given the gradual increase in V_O, one can expect the evolution of Urbach energy (E_U) tails near the CB and VB edges as demonstrated schematically in the inset of Fig. 3(b). However, the key finding is the sudden increase (blue shift) in bandgap at a fluence of 1×10^{17} ions/cm^2 (S_4) up to 3.38 eV as documented in Figs. 3(a) and 3(b). Such a reproducible data can be discussed in two ways: (i) quantum confinement (QC) due to the opening of bandgap below Bohr radius[29] and (ii) B-M effect due to the shift in E_F into the CB for excessive doping of donor electrons.[21,22]

Since the TiO_2 NRs are larger than the Bohr radius (~5 nm) (Ref. 29 and references therein), we can discard the possibility of QC effect to explain the sudden jump in optical bandgap in S_4. On the other hand, the observed blue shift [inset, Fig. 3(b)] can be attributed to uplifting of E_F due to the upsurge of donor electrons with increasing V_O,[28] while degenerate states are formed according to the B-M theory.[21,22] This is further reflected from the UV-VIS-NIR spectrum of S_4 [Fig. 3(a)] revealing a sharp edge due to non-zero occupancy of E_U and the bottom of the CB minimum below E_F following the Pauli exclusion principle.[31] In fact, the width of E_F (ΔE_g) will be proportional to $\frac{n_e^{2/3}}{m_c^*}$, where m_c^* and n_e are the effective mass and concentration of electrons in CB, respectively.[31] In this situation, photon energy required for optical absorption would be more due to the apparent increase in bandgap and becomes higher by an amount of $\left(1+\frac{m_c^*}{m_v^*}\right)\varepsilon$, where m_v^* and ε are the effective mass of holes in VB and electrochemical potential, respectively.[22] Since all defect levels below E_F are occupied in the presence of degenerate states (like in S_4), one would expect to have true bandgap (E_g) when determining E_U using the equation of $\alpha = \alpha_0 \exp\left(\frac{h\nu}{E_U}\right)$, where α is absorption coefficient.[8] To justify it, we have calculated E_U for all fluences as exhibited in the right ordinate of Fig. 3(b), showing that the values for both S_0 and S_4 are almost similar, say 248 and 252 meV, respectively (Fig. S-2).[24] On the other hand, they are 365, 357, and 574 meV for S_1, S_2, and S_3, respectively. Note that α is proportional to $F(R_D)$ in the case of diffused reflectance, while E_U can be determined from the inverse of linear slope of the $\ln[F(R_D)]$ vs $h\nu$ plot.[8]

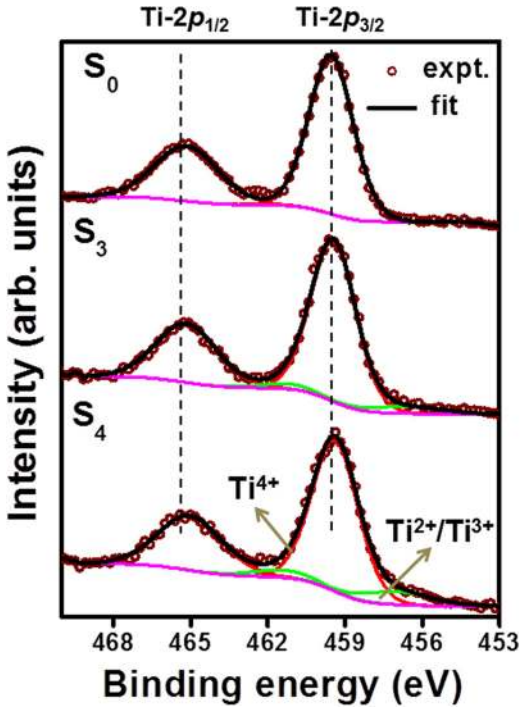

FIG. 4. Typical high-resolution XPS spectra near the Ti-2p region for TiO_2 NRs before (S_0), and after ion beam irradiation with a fluences of 1×10^{16} ions/cm^2 (S_3) and 1×10^{17} ions/cm^2 (S_4). The experimental data are shown by open circles, whereas fitting results are presented by thick black curves. The background subtraction curves are shown in magenta, while the deconvoluted curves for Ti^{4+} and Ti^{2+}/Ti^{3+} are highlighted by red and green colors.

Since surface V_O are expected to participate in forming voids in the sub-surface A-TiO_2 layers,[12] samples were further examined by XPS with increasing ion fluence (Fig. 4). The origin of the oxygen-deficient centers/V_O (due to Ti-O bond breaking[32]) was monitored and interpreted based on quantitative analysis, especially oxidation/valence states of Ti. As it is difficult to follow the change in the Ti $2p_{3/2}$ and $2p_{1/2}$ peaks of S_0, S_3, and S_4, XPS spectra were deconvoluted (Fig. 4) by conventional fitting procedure in Computer Aided Surface Analysis for XPS (CASA-XPS) processing software with Voigt function. The fitting details are summarized in Table I. Careful analysis revealed the appearance of TiO_2 (Ti^{4+}) and TiO/Ti_2O_3 (Ti^{2+}/Ti^{3+}) situated at ~459.5/456.2 eV and 465.2/461.1 eV, respectively.[18] The intermediate phases of TiO/Ti_2O_3 reached the maximum in S_4 with an atomic concentration of ~11.43% by modifying low stability of V_O in the near surface region of A-TiO_2 layer.[5]

TABLE I. XPS fitting parameters showing atomic concentrations of the compositions and corresponding binding energies of Ti $2p_{3/2}$ and $2p_{1/2}$ peaks before and after Ar^+-ion irradiation.

Samples	Oxidation states	Compositions	Components	Binding energy (eV) ± 0.2 eV	Atomic concentration in at. %
S_0	Ti^{4+}	TiO_2	$2p_{3/2}$, $2p_{1/2}$	459.5, 465.2	100
S_1	Ti^{4+}	TiO_2	$2p_{3/2}$, $2p_{1/2}$	459.5, 465.2	92.3
	Ti^{2+}/Ti^{3+}	TiO/Ti_2O_3	$2p_{3/2}$, $2p_{1/2}$	456.5, 461	7.7
S_2	Ti^{4+}	TiO_2	$2p_{3/2}$, $2p_{1/2}$	459.5, 465.3	92.1
	Ti^{2+}/Ti^{3+}	TiO/Ti_2O_3	$2p_{3/2}$, $2p_{1/2}$	456.6, 461.1	7.9
S_3	Ti^{4+}	TiO_2	$2p_{3/2}$, $2p_{1/2}$	459.5, 465.2	91.4
	Ti^{2+}/Ti^{3+}	TiO/Ti_2O_3	$2p_{3/2}$, $2p_{1/2}$	457.1, 461.3	8.6
S_4	Ti^{4+}	TiO_2	$2p_{3/2}$, $2p_{1/2}$	459.4, 465.0	88.6
	Ti^{2+}/Ti^{3+}	TiO/Ti_2O_3	$2p_{3/2}$, $2p_{1/2}$	456.9, 461.4	11.4

In conclusion, we report 50 keV Ar^+-ion induced modification of optical bandgap in self-assembled TiO_2 NRs on Si pyramids at RT. This showed a transformation from the crystalline to amorphous TiO_2 layer with increasing fluence from 5×10^{14} to 1×10^{17} ions/cm^2. A systematic decrease in bandgap from 3.23 to 2.94 eV up to a fluence of 1×10^{16} ions/cm^2 was found to be increased suddenly to 3.38 eV at 1×10^{17} ions/cm^2. The latter one was correlated with the evolution of voids through accumulation of V_O. The decrease in bandgap was discussed in the light of introduction of defect states, while increasing bandgap at 1×10^{17} ions/cm^2 was associated with the degenerate states according to Burstein-Moss effect. We believe that the present intriguing phenomenon is promising for controlled applications in both photocatalytic and optoelectronic devices by judicial use of the energetic Ar^+ ions.

The authors would like to acknowledge the help received from the scientists at Inter-University Accelerator Centre, New Delhi, and Dr. P. K. Sahoo from National Institute of Science Education and Research, Bhubaneswar, for ion irradiation and SEM measurements, respectively.

[1]C. M. Yim, C. L. Pang, and G. Thornton, Phys. Rev. Lett. **104**, 036806 (2010).
[2]R. Fernandes, N. Patel, R. Dholam, M. Adami, and A. Miotello, Surf. Coat. Technol. **203**, 2579 (2009).
[3]M. M. Khan, S. A. Ansari, D. Pradhan, M. O. Ansari, D. H. Han, J. Lee, and M. H. N. Cho, J. Mater. Chem. A **2**, 637 (2014).
[4]H. Seo, A. B. Posadas, C. Mitra, A. V. Kvit, J. Ramdani, and A. A. Demkov, Phys. Rev. B **86**, 075301 (2012).
[5]H. Cheng and A. Selloni, Phys. Rev. B **79**, 092101 (2009).
[6]D. O. Scanlon, C. W. Dunnill, J. Buckeridge, S. A. Shevlin, A. J. Logsdail, S. M. Woodley, C. R. A. Catlow, M. J. Powell, R. G. Palgrave, I. P. Parkin, G. W. Watson, T. W. Keal, P. Sherwood, A. Walsh, and A. A. Sokol, Nat. Mater. **12**, 798 (2013).
[7]J. Liu, P. M. Hosseinpour, S. Luo, D. Heiman, L. Menon, D. A. Arena, and L. H. Lewis, J. Vac. Sci. Technol. **33**, 021202 (2015).
[8]B. Choudhury, M. Dey, and A. Choudhury, Int. Nano Lett. **3**, 25 (2013).
[9]C. Dette, M. A. Pérez-Osorio, C. S. Kley, P. Punke, C. E. Patrick, P. Jacobson, F. Giustino, S. J. Jung, and K. Kern, Nano Lett. **14**, 6533 (2014).
[10]D. Kan, T. Terashima, R. Kanda, A. Masuno, K. Tanaka, S. Chu, H. Kan, A. Ishizumi, Y. Kanemitsu, Y. Shimakawa, and M. Takano, Nat. Mater. **4**, 816 (2005).
[11]S. Wendt, P. T. Sprunger, E. Lira, G. K. H. Madsen, Z. Li, J. Ø. Hansen, J. Matthiesen, A. Blekinge-Rasmussen, E. Lægsgaard, B. Hammer, and F. Besenbacher, Science **320**, 1755 (2008).
[12]P. Scheiber, M. Fidler, O. Dulub, M. Schmid, U. Diebold, W. Hou, U. Aschauer, and A. Selloni, Phys. Rev. Lett. **109**, 136103 (2012).
[13]Y. He, O. Dulub, H. Cheng, A. Selloni, and U. Diebold, Phys. Rev. Lett. **102**, 106105 (2009).
[14]U. Aschauer, Y. He, H. Cheng, S.-C. Li, U. Diebold, and A. Selloni, J. Phys. Chem. C **114**, 1278 (2010).
[15]D. Leong, M. Harry, K. J. Reeson, and K. P. Homewood, Nature **387**, 686 (1997).
[16]T. Luttrell, W.-K. Li, X.-Q. Gong, and M. Batzill, Phys. Rev. Lett. **102**, 166103 (2009); P. Karmakar, G. F. Liu, and J. A. Yarmoff, Phys. Rev. B **76**, 193410 (2007).
[17]B. M. Pabón, J. I. Beltrán, G. Sánchez-Santolino, I. Palacio, J. López-Sánchez, J. Rubio-Zuazo, J. M. Rojo, P. Ferrer, A. Mascaraque, M. C. Muñoz, M. Varela, G. R. Castro, and O. Rodríguez de la Fuente, Nat. Commun. **6**, 6147 (2015).
[18]A. Barman, C. P. Saini, P. Sarkar, B. Satpati, S. R. Bhattacharyya, D. Kabiraj, D. Kanjilal, S. Dhar, and A. Kanjilal, J. Appl. Phys. **118**, 224903 (2015).
[19]S. Chhajed, M. F. Schubert, J. K. Kim, and E. F. Schubert, Appl. Phys. Lett. **93**, 251108 (2008).
[20]C. P. Saini, A. Barman, M. Kumar, P. K. Sahoo, T. Som, and A. Kanjilal, Appl. Phys. Lett. **105**, 123901 (2014).
[21]J. Yao, K. J. Koski, W. Luo, J. J. Cha, L. Hu, D. Kong, V. K. Narasimhan, K. Huo, and Yi. Cui, Nat. Commun. **5**, 5670 (2014).
[22]M. G. Zachary, L. Aaron, and G. J. Snyder, New J. Phys. **15**, 075020 (2013).
[23]J. F. Ziegler, M. D. Ziegler, and J. P. Biersack, Nucl. Instrum. Methods B **268**, 1818 (2010).
[24]See supplementary information at http://dx.doi.org/10.1063/1.4939662 for showing the vacancies distribution with TiO_2 thickness as determined by SRIM calculations and Urbach energy plots for different ion fluences.
[25]D. P. Singh and J. P. Singh, Appl. Phys. A **114**, 1189 (2014).
[26]E. S. Andrés, M. Toledano-Luque, A. del Prado, M. A. Navacerrada, I. Mártil, G. González-Díaz, W. Bohne, J. Röhrich, and E. Strub, J. Vac. Sci. Technol. **23**, 1523 (2005).
[27]T. Basu, M. Kumar, S. Nandy, B. Satpati, C. P. Saini, A. Kanjilal, and T. Som, J. Appl. Phys. **118**, 104903 (2015).
[28]U. Diebold, Surf. Sci. Rep. **48**, 53 (2003).
[29]H. Lin, C. P. Huang, W. Li, C. Ni, S. I. Shah, and Y.-H. Tseng, Appl. Catal. B **68**, 1 (2006).
[30]M. Batzill, E. H. Morales, and U. Diebold, Phys. Rev. Lett. **96**, 026103 (2006).
[31]R. Eisele, N. J. Blumenstein, J. Baier, S. Walheim, T. Schimmel, and J. Bill, CrystEngComm **16**, 1560 (2014).
[32]E. McCafferty and J. P. Wightman, Appl. Surf. Sci. **143**, 92 (1999); M. Ramamoorthy, R. D. King-Smith, and D. Vanderbilt, Phys. Rev. B **49**, 7709 (1994).